

Scale-Variant Robust Kernel Optimization for Non-linear Least Squares Problems

Shounak Das¹ and Jason Gross¹

¹Department of Mechanical and Aerospace Engineering , West Virginia University , Morgantown, USA

Abstract—In this letter, we present an algorithm for iterative nonlinear least squares which increases the adaptive nature of previous methods in the literature. Our method uses two parameters to learn the best fitting distribution of the measurement residuals and performs Iterative Re-weighted Least Squares (IRLS) based on these two parameters. This adaptive nature of the weights is shown to be helpful in situations where the noise level varies in the measurements, and is shown to increase robustness to outliers. We test our algorithm first on the point cloud registration problem with synthetic data sets, where the truth transformation is known. Next, we also evaluate the approach with an open-source LiDAR-inertial SLAM package to demonstrate that the proposed approach is more effective than constant parameters for the application of incremental LiDAR-inertial odometry. This increased adaptivity can help in a wide range of estimation problems in robotics by better modelling the measurement errors.

Index Terms—Robust estimation, point cloud registration, adaptive loss, iterative non-linear least squares

I. INTRODUCTION

Robustness is a very important property that is necessary for any estimation algorithm running on robotic systems. In any real-world scenario, noise levels fluctuate and sensor data gets corrupted by outliers (e.g., multipath reflections and jamming attacks in GNSS [1], presence of wrong correspondences or dynamic objects in registration problems [2], slippage in wheel odometry data [3], dark or shaded areas in visual odometry). Current state-of-the-art methods try to detect these harmful scenarios and can either remove [4] or de-weight the suspected “bad” measurements [5]. In this article, the focus is on the de-weighting approach. First, we overview the literature and provide a description of previous works from which the proposed approach draws inspiration. Next, the proposed algorithm is described along with the intuition behind it. Lastly, the proposed method is compared with other well-known approaches with respect to estimation performance using both synthetic data and real-world scenarios.

II. LITERATURE REVIEW

Robust estimation aims at estimating the correct parameters with or without the presence of measurements errors that vary from the expected distribution (i.e., typically assumed Gaussian). Many of the modern robust estimation techniques used in robotics draw inspiration from works of Huber [6], Tukey [7], Hampel [8] in the field of robust statistics. Bosse et al. [9] gives brief, but accurate, descriptions of these

statistical concepts called M-estimators and their applications to robotics. The importance of M-estimators in point cloud registration and visual navigation have been discussed in [10] [11]. The proposed algorithm uses a generalized version of these M-estimators developed by Barron [12] and extended by Chebrolu [2]. M-estimators fall within the de-weighting group of methods, which don’t directly remove measurements. The intuition behind this is that, instead of assuming a Gaussian distribution for the measurement noise, these M-estimators have heavier tails, which solve for the parameters that best fit the overall data. An interesting connection between M-estimators and elliptical distributions was shown in [13], which was used for parameter estimation. The cost functions obtained from negative log-likelihood of these distributions are modified versions of the squared loss function, which are optimized to get to the correct solution. Some of these functions are non-convex and suffer from the local minima problem (eg. Redescending M-estimators). To tackle this, [5] uses the concepts of graduated non-convexity, along with the Black-Rangarajan duality [14], to devise an iterative algorithm for robust perception.

The other group of the robust estimation methods focus on the finding the maximum number of measurements that satisfy a specific inlier condition, which is also called the Maximum Consensus (MC) problem [15]. One of the most well-known methods to solve these kind of problems is called Random Sample Consensus (RANSAC) [16]. Numerous variations of this algorithms have been developed [17], and still remains an important area of research. Antonante et al. [18] provides in-depth discussion of various robust estimation methods across different disciplines along with their computational limits. They develop minimally tuned algorithms that can tolerate large number of outliers. Shi et al. [4] uses invariance relations between measurements to solve MC problems by converting it into a maximal clique problem.

III. M-ESTIMATORS AND LEAST-SQUARES

M-estimation [9] replaces the standard squared loss function by a function which reduces the effect of measurements with large residuals. This is a continuous optimization problem, which can be solved iteratively with gradient descent .

$$\theta^* = \underset{\theta}{\operatorname{argmin}} \sum_{i=1}^N \rho(x_i(\theta)). \quad (1)$$

Equation 1 can be solved by looking at how general (un-weighted or weighted) nonlinear least square problems are solved.

$$\hat{\theta} = \arg \min_{\theta} \sum_{i=1}^N \|\mathbf{x}_i(\theta)\|^2.$$

$$\hat{\theta}_w = \arg \min_{\theta} \sum_{i=1}^N w_i \|\mathbf{x}_i(\theta)\|^2.$$

Two families of methods are used generally: line search methods (e.g., Gauss-Newton) and trust region methods (e.g., Levenberg-Marquardt), both of which are iterative descent methods [19] [20]. Partially differentiating the least squares and M-estimation expressions in their scalar forms with respect to the unknown parameter θ shows

$$\frac{1}{2} \frac{\partial (w_i x_i^2(\theta))}{\partial \theta} = w_i x_i(\theta) \frac{\partial x_i(\theta)}{\partial \theta}$$

$$\frac{\partial (\rho(x_i(\theta)))}{\partial \theta} = \rho'(x_i(\theta)) \frac{\partial x_i(\theta)}{\partial \theta}.$$

Comparing these two expressions, it is apparent that M-estimation can be solved exactly like a weighted nonlinear least squares problem. The weights in this case is given by

$$w_i = \frac{\rho'(x_i(\theta))}{x_i(\theta)}.$$

Hence this method of solving M-estimation problems is called Iterative Re-weighted Least Squares (IRLS) [9].

IV. ONE FUNCTION FOR ALL

In this letter, the approach starts with Barron's work on unifying different robust cost functions in [12].

$$\rho(x, \alpha, c) = \begin{cases} \frac{1}{2}(x/c)^2 & \text{if } \alpha = 2 \\ \log(\frac{1}{2}(x/c)^2 + 1) & \text{if } \alpha = 0 \\ 1 - \exp(-\frac{1}{2}(x/c)^2) & \text{if } \alpha = -\infty \\ \frac{|\alpha-2|}{\alpha} \left(\left(\frac{(x/c)^2}{|\alpha-2|} + 1 \right)^{\alpha/2} - 1 \right) & \text{otherwise} \end{cases} \quad (2)$$

This form of cost function is convenient because different variations of M-estimators can be expressed by changing the parameter α . x is the residual value depending on the estimation problem at hand. c is sometimes referred to as the scale parameter. This article aims to understand the effects of changing α and c values in different robust estimation scenarios. As described earlier, M-estimators de-weight suspected outlier residuals instead of removing them completely. This is helpful in cases where removing data can affect the solution accuracy. The weight depends on the derivative $\frac{\partial \rho}{\partial x}$ and the residual x . The partial derivatives of this cost function with respect to x is given below.

$$\frac{\partial \rho}{\partial x}(x, \alpha, c) = \begin{cases} \frac{x}{c^2} & \text{if } \alpha = 2 \\ \frac{2x}{x^2 + 2c^2} & \text{if } \alpha = 0 \\ \frac{x}{c^2} \exp(-\frac{1}{2}(x/c)^2) & \text{if } \alpha = -\infty \\ \frac{x}{c^2} \left(\frac{(x/c)^2}{|\alpha-2|} + 1 \right)^{(\alpha/2-1)} & \text{otherwise} \end{cases} \quad (3)$$

The sum of cost of the all residuals can be optimized to solve for the unknown state

$$\hat{X} = \arg \min_{\theta, \alpha, c} \sum_i \rho(x_i(\theta), \alpha, c). \quad (4)$$

A better understanding of the optimization problem can be obtained by looking at the partial derivatives of ρ with respect to α and c .

$$\frac{\partial \rho}{\partial \alpha}(x, \alpha, c) \geq 0 \quad (5)$$

$$\frac{\partial \rho}{\partial c}(x, \alpha, c) \leq 0 \quad \text{if } c \geq 0. \quad (6)$$

Since ρ in equation 2 is even with respect to c , only positive values for c are used. Equations 5 and 6 show the cost decreases with decreasing α when c is constant. It also decreases when c increases with constant α . Fig. 1 shows how the weights depend on α and c . The problem of optimizing equation 4 with respect to (x, α) or (x, c) is that, in both cases, the solution will trivially move towards lower values of α and higher values of c , thus not representing the true distribution of the residuals and, in turn, affecting the estimates of the unknown parameters. Barron et al. [12] removes this issue by assuming a distribution given by

$$P_*(x, \alpha, c) = \frac{1}{cZ(\alpha)} e^{-\rho(x, \alpha, c)}$$

$$Z(\alpha) = \int_{-\infty}^{\infty} e^{-\rho(x, \alpha, 1)} dx. \quad (7)$$

This creates a shifted version of cost function. Using negative log-likelihood we get

$$\rho_*(x, \alpha, c) = \rho(x, \alpha, c) + \log(cZ(\alpha)). \quad (8)$$

With this, whenever ρ_* is optimized with respect to (x, α) , the solution cannot trivially go to the least value of α due to the newly added penalty term. The optimization process attempts to balance between the lower cost of larger residuals and the higher cost of the inliers. However, another problem arises with this shifted expression, which is that $Z(\alpha)$ is unbounded for negative values of α . Thus the optimization cannot be done in the negative domain of α , which is not ideal because negative α values can be useful in presence of large residuals. Chebrolu et al. [2] used a truncated version of $Z(\alpha)$ to circumvent this issue

$$\hat{Z}(\alpha) = \int_{-\tau}^{\tau} e^{-\rho(x, \alpha, 1)} dx. \quad (9)$$

$\hat{Z}(\alpha)$ can be calculated for both positive and negative values of α . The only assumption with this formulation is that any residual with magnitude greater than τ has zero probability. Replacing $Z(\alpha)$ with $\hat{Z}(\alpha)$, P_* and Z_* is shown in Fig. 2. Instead jointly optimizing over (x, α, c) , [2] first finds the α that has the lowest negative log-likelihood with the current residuals, and then solves equation 4 with iterative re-weighted least squares with this last optimal value of α . These two steps are repeated until convergence is achieved. c is kept constant in this method, usually set to 1. The algorithm is described in 1, θ is the vector of parameters to be estimated. This algorithm is referred to in this letter as RKO.

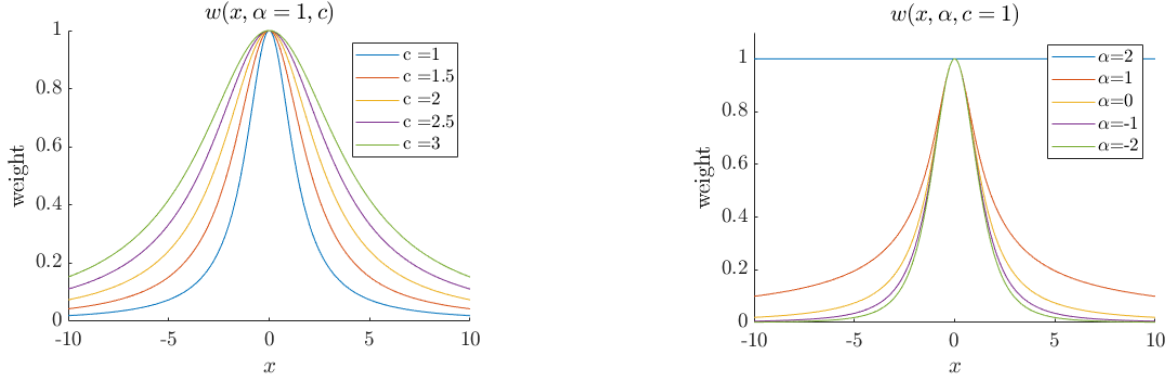


Fig. 1: Left : weights as a function of residuals and c with constant α , Right : weights as a function of residuals and α with constant c

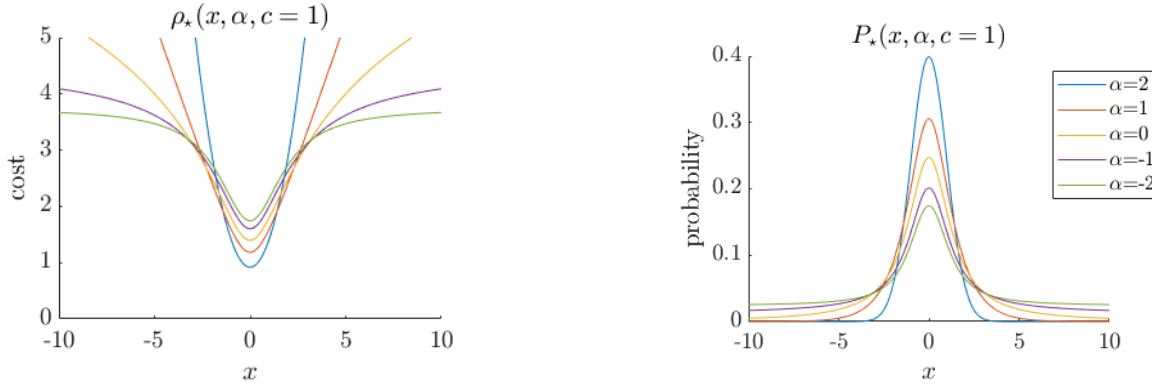


Fig. 2: Left : shifted cost as a function of residual and α using truncated $Z(\alpha)$, Right : shifted distribution as a function of residual and α using truncated $Z(\alpha)$

Algorithm 1 Robust Kernel Optimization (RKO) [2]

Initialize $\theta^0 = \theta, \alpha^0, c$
 while !converged do
 Step 1: Minimize for α
 $\alpha^t = \operatorname{argmin}_{\alpha} - \sum_{i=1}^N \log P_*(x_i(\theta^{t-1}), \alpha^{t-1}, c)$
 Step 2: Minimize robust loss using IRLS
 $\theta^t = \operatorname{argmin}_{\theta} \sum_{i=1}^N \rho(x_i(\theta), \alpha^t, c),$
 end while

V. SCALE-VARIANT ROBUST KERNEL OPTIMIZATION

Algorithm 1 has been shown to work well for LiDAR SLAM in the presence of dynamic objects as well as bundle adjustment [2]. However, in the work herein, finding a way to adapt c along with x , α is considered for the purpose of yielding further improvements in such situations. To that end, a slightly different variation of the probability distribution \hat{P} is proposed

$$\hat{P}(x, \alpha, c) = \frac{1}{\hat{Z}(\alpha, c)} e^{-\rho(x, \alpha, c)} \quad (10)$$

$$\hat{Z}(\alpha, c) = \int_{-\tau}^{\tau} e^{-\rho(x, \alpha, c)} dx.$$

Similar to the shifted cost above, the cost corresponding to this distribution is obtained by taking the negative log-likelihood

$$\hat{\rho}(x, \alpha, c) = \rho(x, \alpha, c) + \log(\hat{Z}(\alpha, c)). \quad (11)$$

The behavior of this probability distribution can be understood by looking at Fig. 3. In the left graph \hat{P} shows behavior similar to the P_* , where in the presence of large noise or outliers, α decreases and thus creates a more heavy-tailed distribution, with probability mass moving from the smaller residuals towards the larger residuals. But there is not a lot of probability change for the mid-range residuals (i.e., values close to 3 and 4). This is where the advantage of \hat{P} over P_* can be understood. The right graph in Fig. 3 shows increasing c with a constant α moves probability mass from the smaller residuals to the mid-range residuals and minimal change in probability for larger magnitudes. This can be useful in the presence of varying noise levels, for example, reducing α with constant c would help for larger noise or outlier levels, however, in the presence of lower noise levels, increasing c with constant α can be more beneficial. Essentially, \hat{P} gives an additional “degree of freedom” of better fitting the existing residuals by adapting c along with α . From a weight perspective, a similar concept can be seen in Fig. 1. When decreasing α with constant c , the weight drops quite fast from the lower to mid-range residuals but then flattens out at larger residuals. However, when increasing c with α constant, the weight changes at a much slower rate. Thus, with the addition of changing c , the optimization explores more values in the weight space which helps the IRLS step. Note for $\alpha = 2$, changing c does not change the weights, they all remain 1. This is because changing c only changes the variance for the

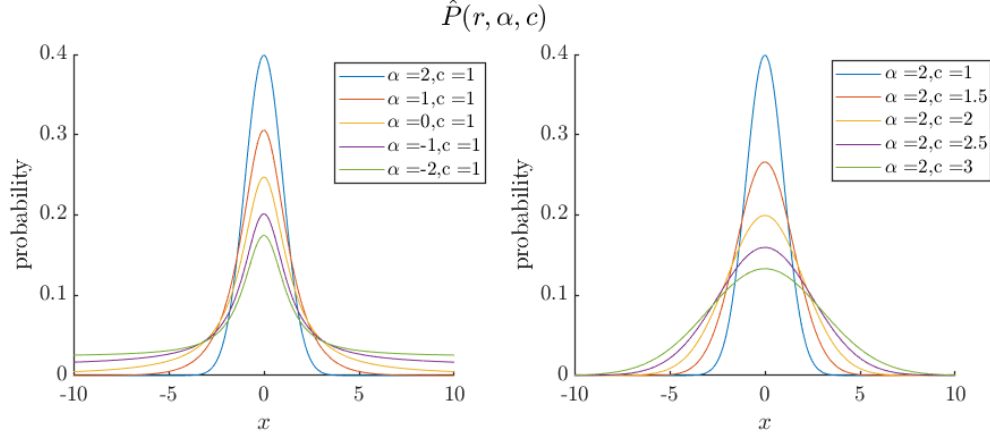


Fig. 3: Proposed probability distribution \hat{P} with two variations: changing α and constant c (left); constant α and changing c (right).

Gaussian distribution.

Now, given Algorithm 1, another step can easily be added in this method, where, after minimizing the log-likelihood with respect to α , the log-likelihood with respect to c is minimized. We call this the Scale-variant Robust Kernel Optimization (S-RKO) method. The steps of this algorithm are shown in Algorithm 2. It is very similar to the original algorithm. It starts with initial guesses θ^0 , α^0 and c^0 . Then for any time step t the following steps are conducted: first, with the current value of c^{t-1} , and the residuals $x(\theta^{t-1})$, find α^t that minimizes the negative log-likelihood of the residuals. This can be done easily with grid search. Then, c^t is obtained by minimizing the negative log-likelihood that is calculated with $x(\theta^{t-1})$ and α^t . Lastly, with α^t and c^t , the loss function in equation 4 can be optimized iteratively using Gauss-Newton method. In steps 1 and 2 of this algorithm, in order to search for optimum values of α and c we discretize over their possible ranges. A pre-computed table of values of $\hat{Z}(\alpha, c)$ is used for each of the grid searches.

Algorithm 2 Scale-variant Robust Kernel Optimization (S-RKO)

```

Initialize  $\theta^0 = \theta, \alpha^0, c^0$ 
while !converged do
  Step 1: Minimize for  $\alpha$ 
   $\alpha^t = \operatorname{argmin}_{\alpha} - \sum_{i=1}^N \log \hat{P}(x_i(\theta^{t-1}), \alpha^{t-1}, c^{t-1})$ 
  Step 2: Minimize for  $c$ 
   $c^t = \operatorname{argmin}_c - \sum_{i=1}^N \log \hat{P}(x_i(\theta^{t-1}), \alpha^t, c^{t-1})$ 
  Step 3: Minimize robust loss using IRLS
   $\theta^t = \operatorname{argmin}_{\theta} \sum_{i=1}^N \rho(x_i(\theta), \alpha^t, c^t)$ 
end while

```

VI. EXPERIMENTS

A. Synthetic Data

First, the proposed algorithm S-RKO is tested for pairwise point cloud registration problem with the open source implementation and synthetic range data sets provided in [21]. The registration algorithm of [21], referred to in the article as FastReg, rewrites the scaled Geman-McClure estimator as an outlier process using Black-Rangarajan duality [14] and

solves it iteratively. Since this cost function is non-convex, to avoid local minima the method starts with a convex version of this function and change the scale parameter after every few iterations to increase the non-convexity. The RMS values for the given 25 range data sets are compared in Fig. 4. We refer the readers to [21] for details about these data sets which come from AIM@SHAPE repository, the Berkeley Angel dataset and the Stanford 3D Scanning repository.

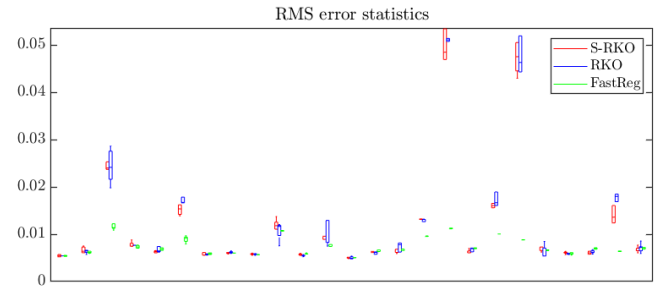


Fig. 4: RMS error statistics (Y axis) over 10 trials for 25 synthetic range data sets (X axis)

B. Real world data

Next, the proposed algorithm is tested within the LiDAR-inertial SLAM package LIO-SAM [22]. Four of openly available datasets (*campus(small)*, *garden*, *park*, *rotation*) are used for evaluation. Unlike the Fast Point Feature Histogram (FPFH) features [23] used in FastReg, LIO-SAM uses corner and surface features of the LiDAR point cloud for odometry based on the well-known LiDAR SLAM method LOAM [24]. Before discussing the results, it is important to understand how S-RKO and RKO were implemented inside the LiDAR odometry module of LIO-SAM. For LiDAR odometry, corner and surface features extracted from the current time-step's point cloud is then registered with corner and surface features of the n last keyframes in the map. Correspondences between the features of current scan and map is found using a nearest neighbour Kd-tree search. In the proposed implementation, the

residuals used for learning α and c are the distances between these feature correspondences.

$$x_{\text{corner/surface}} = \|p_{\text{map}} - q_{\text{current}}\|_2, \quad (12)$$

where p and q are features in the map and current scan respectively. The nonlinear least squares in LIO-SAM only accepts features whose distances from their correspondences are less than 1. In this setup, the parameters of RKO and S-RKO do not change from $\alpha = 2$, $c = 1$, which results in equal weighting of all the features. Here, this is changed to accept correspondences with larger distances. In this way, other parameter values are learned and the weights can change accordingly. This change however does make it harder for the algorithms since possibly wrong correspondences are let into the nonlinear least squares estimation. The objective, in this case, is to see if allowing these large residuals and de-weighting them can perform comparably with removing them.

VII. RESULTS AND DISCUSSION

For the algorithm implementations of RKO and S-RKO, values for $\hat{Z}(\alpha, c)$ with τ values set to 10 are calculated, meaning it is assumed that there are no residuals with magnitude greater than 10. For synthetic data sets, RKO is initialized with $\alpha^0 = 0$ and $c^0 = 1$ and S-RKO with $\alpha^0 = 0$ and $c^0 = 3.5$. It was determined that the parameters always converge to $\alpha = 2$, $c = 1$ for both RKO and S-RKO. Ten trials are done for each algorithm for each data and the statistics are shown in Fig. 4. For most of the data sets, the performance of S-RKO compares well with FastReg, however, FastReg outperforms both S-RKO and RKO by a large margin for two of them. In general, S-RKO performs comparably with RKO and FastReg.

For the LIO-SAM implementation, four algorithms are compared : S-RKO; RKO; a version where larger residuals are let in and α , c are kept constant; and lastly the standard LIO-SAM algorithm, where all large residuals are removed. RKO and S-RKO are evaluated with respect to LIO-SAM without GPS. Other performance parameters are calculated such as the number of keyframes tracked and the quality of generated map. Other than the LIO-SAM implementation, which is used as the ground truth, loop closures were disabled. RKO was initialized with $\alpha^0 = 1.5$ and $c^0 = 1.5$; S-RKO with $\alpha^0 = 1.5$ and $c^0 = 1$, and the constant parameter version with $\alpha^0 = 2$ and $c^0 = 1$. The discretized range of α values come from $\{-8 : 0.25 : 2\}$ and c values come from $\{1 : 0.25 : 6\}$, where the first and last values are the limits and middle value is the step. We chose initialization parameters close to $\alpha = 2$ and $c = 1$ because initialization values further from these values made both RKO and S-RKO unstable since the registration is not able to converge in real-time.

The first result with LIO-SAM is with the *rotation* data which is translationally static but has multiple fast rotational motions. This data was found to be hardest for the algorithms S-RKO and RKO, resulting in divergences in some trials, mainly due to the frequency of the fast rotations. In general, the generated map of RKO was found to be slightly better than S-RKO (Fig. 5 and Fig. 6). The map generated by the

constant parameter version was noisier than both S-RKO and RKO.

Tables I and II show RMS errors with respect to the standard LIO-SAM implementation and number of keyframes tracked for the *park* and *campus(small)* datasets. Due to acceptance of large outliers, RKO and S-RKO are able to track lesser number of keyframes, but still able to find solutions close to LIO-SAM. The constant parameter version is able to track the least number of keyframes in both data sets resulting in tracking loss in some parts of the trajectories. The larger RMS error for RKO as compared to the constant parameter version in *campus(small)* data is caused by poor registration towards the beginning of the trajectory, as shown in Fig. 7. Looking at the learned parameters of S-RKO for *campus(small)* data, Fig. 8, it is shown that α has its lowest values in the section of the trajectory where there are cars moving nearby (i.e., the region pointed at by the arrow). This is similar to what is reported by [2] for Kitti data. This is due to increased robustness with lower values of α which helps to maintain tracking. Fig. 9 shows the S-RKO map and trajectory at that time frame in the *park* data.

TABLE I: RMS errors (m) with respect to LIO-SAM

	const. params	RKO	S-RKO
<i>park</i>	11.72	2.27	2.99
<i>campus(small)</i>	1.02	3.38	0.66

* Best performance in bold.

TABLE II: Number of keyframes tracked (larger is better)

	const. params	RKO	S-RKO	LIO-SAM
<i>park</i>	488	609	568	787
<i>campus(small)</i>	326	380	392	543

* Best performance in bold.

Lastly, the results for the *garden* data are shown. This data also has some instances of fast rotations along with fast translations. Both the constant parameter approach and the RKO approach fail in such a condition, however, the proposed S-RKO approach is able to generate the map properly, as shown in Fig. 10 and Fig. 11. This could be due to the less aggressive weighting that S-RKO can achieve but that RKO cannot. The learned parameters of S-RKO for this data, Fig. 12, shows that α is the lowest in of the sections of large rotations and translations, pointing again to increased robustness. In the joint space of (α, c) , most of the epochs the values are found to center around $(2, 1)$, which represents the standard Gaussian($\mu = 0$, $\sigma^2 = 1$). α values will only decrease from 2 to increase robustness and usually coincide with c values close to 1. c values will always increase from 1 and mostly coincide with α values close to 2. This suggests decreasing α mainly helps during aggressive rotations or translations or presence of dynamic objects and increasing c helps in low noise scenarios where the noise distribution is close to Gaussian. For better understanding of the joint variability of α and c , more testing is needed.

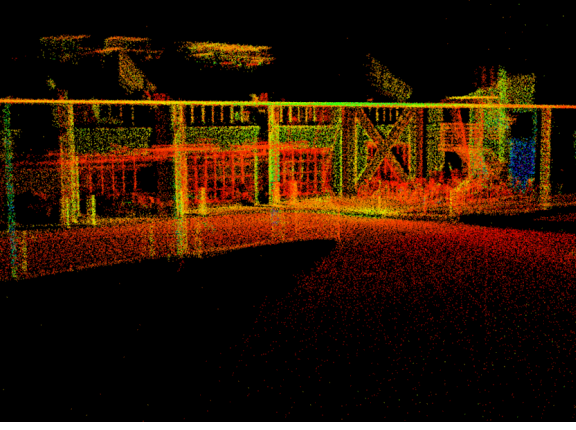


Fig. 5: RKO map generated with *rotation* data

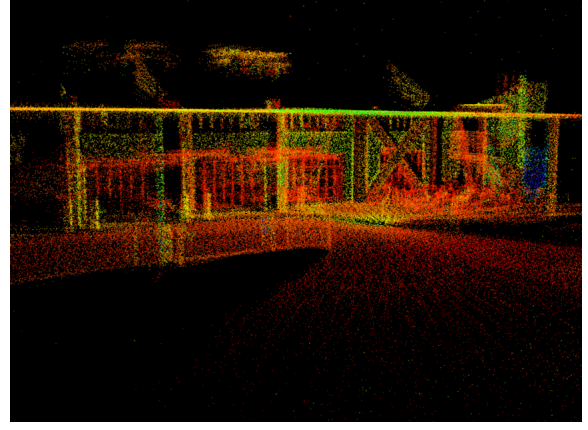


Fig. 6: S-RKO map generated with *rotation* data

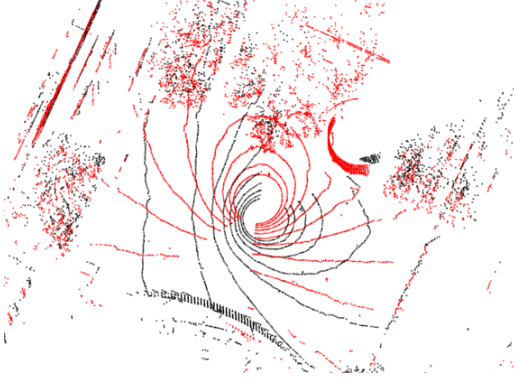


Fig. 7: Incorrect registration in RKO between local map(black) and current scan(red) towards the beginning of campus trajectory. S-RKO did not have any such issues.

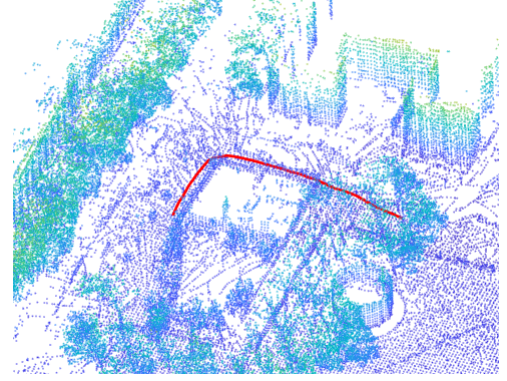


Fig. 9: Section of the *campus* map and trajectory created by S-RKO where moving cars are present

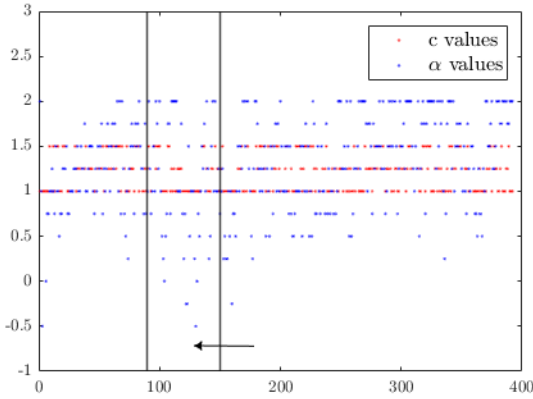


Fig. 8: S-RKO parameter variation along *campus(small)* data. The region pointed by the arrow is the only part of the trajectory which scans moving cars.

VIII. CONCLUSION AND FUTURE WORK

In this paper we develop and implement an extended version of the algorithm described in [2], which gives more adaptivity to the IRLS method. We show both the original algorithm and extended version perform well for LiDAR odometry in different scenarios. We also show low values of α in our

algorithm point to presence of dynamic objects nearby or large rotational and translational motions. Adaptivity in c mainly helps in low noise scenarios and helps explore more of the weight space during nonlinear least squares. Future work will focus on their performances in presence of large number of dynamic objects. This algorithm can also be tested on other estimation problems due to the ubiquity of nonlinear least squares problems.

REFERENCES

- [1] J. N. Gross, C. Kilic, and T. E. Humphreys, "Maximum-likelihood power-distortion monitoring for gnss-signal authentication," *IEEE Transactions on Aerospace and Electronic Systems*, vol. 55, no. 1, pp. 469–475, 2018.
- [2] N. Chebrolu, T. Labe, O. Vysotska, J. Behley, and C. Stachniss, "Adaptive robust kernels for non-linear least squares problems," *IEEE Robotics and Automation Letters*, vol. 6, no. 2, pp. 2240–2247, 2021.
- [3] C. Kilic, N. Ohi, Y. Gu, and J. N. Gross, "Slip-based autonomous zupt through gaussian process to improve planetary rover localization," *IEEE Robotics and Automation Letters*, vol. 6, no. 3, pp. 4782–4789, 2021.
- [4] J. Shi, H. Yang, and L. Carlone, "Robin: a graph-theoretic approach to reject outliers in robust estimation using invariants," in *2021 IEEE International Conference on Robotics and Automation (ICRA)*. IEEE, 2021, pp. 13 820–13 827.
- [5] H. Yang, P. Antonante, V. Tzoumas, and L. Carlone, "Graduated non-convexity for robust spatial perception: From non-minimal solvers to global outlier rejection," *IEEE Robotics and Automation Letters*, vol. 5, no. 2, pp. 1127–1134, 2020.
- [6] P. J. Huber, *Robust statistics*. John Wiley & Sons, 2004, vol. 523.

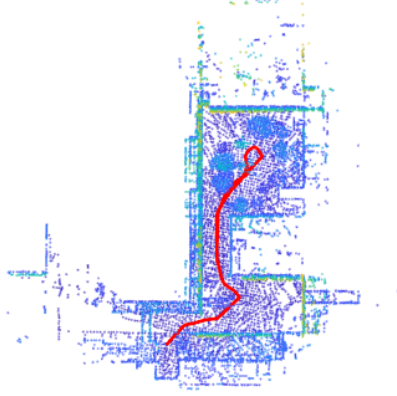


Fig. 10: *Garden map generated with RKO. RKO failed at the first instance of large translations and rotations and could not generate the whole map.*

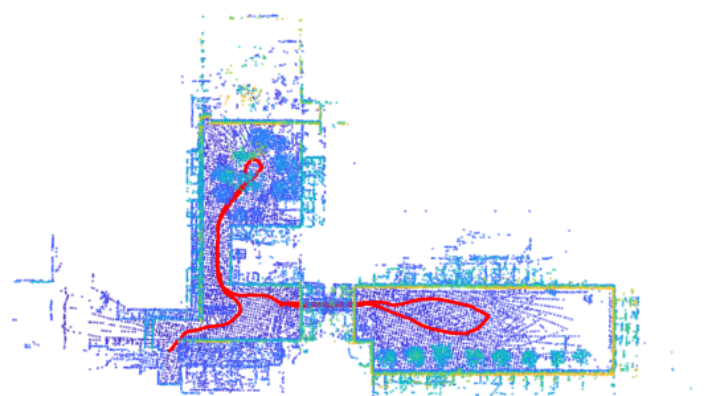


Fig. 11: *Garden map generated with S-RKO. S-RKO was able to maintain tracking during the two instances of large motions (near the two loops) and create a better map.*

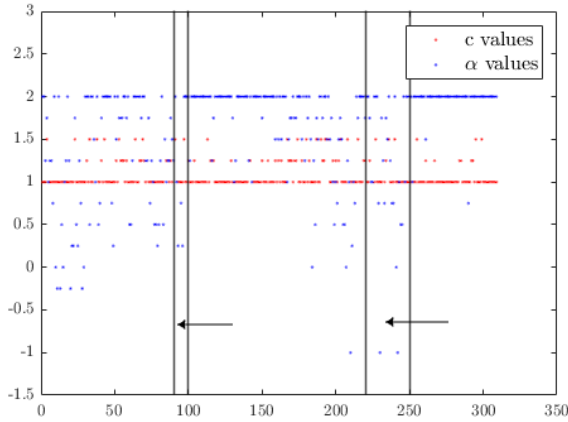


Fig. 12: *S-RKO parameter variation along garden data. The regions pointed by the arrows show the instances of large translational/rotational motions.*

- [7] —, “John w. tukey’s contributions to robust statistics,” *Annals of statistics*, pp. 1640–1648, 2002.
- [8] F. R. Hampel, E. M. Ronchetti, P. J. Rousseeuw, and W. A. Stahel, *Robust statistics: the approach based on influence functions*. John Wiley & Sons, 2011, vol. 196.
- [9] M. Bosse, G. Agamennoni, I. Gilitschenski *et al.*, *Robust estimation and applications in robotics*. Now Publishers, 2016.
- [10] P. Babin, P. Giguere, and F. Pomerleau, “Analysis of robust functions for registration algorithms,” in *2019 International Conference on Robotics and Automation (ICRA)*. IEEE, 2019, pp. 1451–1457.
- [11] K. MacTavish and T. D. Barfoot, “At all costs: A comparison of robust cost functions for camera correspondence outliers,” in *2015 12th conference on computer and robot vision*. IEEE, 2015, pp. 62–69.
- [12] J. T. Barron, “A general and adaptive robust loss function,” in *Proceedings of the IEEE/CVF Conference on Computer Vision and Pattern Recognition*, 2019, pp. 4331–4339.
- [13] G. Agamennoni, P. Furgale, and R. Siegwart, “Self-tuning m-estimators,” in *2015 IEEE International Conference on Robotics and Automation (ICRA)*. IEEE, 2015, pp. 4628–4635.
- [14] M. J. Black and A. Rangarajan, “On the unification of line processes, outlier rejection, and robust statistics with applications in early vision,” *International journal of computer vision*, vol. 19, no. 1, pp. 57–91, 1996.
- [15] T.-J. Chin and D. Suter, “The maximum consensus problem: recent

algorithmic advances,” *Synthesis Lectures on Computer Vision*, vol. 7, no. 2, pp. 1–194, 2017.

- [16] M. A. Fischler and R. C. Bolles, “Random sample consensus: a paradigm for model fitting with applications to image analysis and automated cartography,” *Communications of the ACM*, vol. 24, no. 6, pp. 381–395, 1981.
- [17] M. Zuliani, “Ransac for dummies,” *Vision Research Lab, University of California, Santa Barbara*, 2009.
- [18] P. Antonante, V. Tzoumas, H. Yang, and L. Carlone, “Outlier-robust estimation: Hardness, minimally tuned algorithms, and applications,” *IEEE Transactions on Robotics*, 2021.
- [19] K. Madsen, H. Nielsen, and O. Tingleff, “Methods for non-linear least squares problems (2nd ed.),” p. 60, 01 2004.
- [20] H. P. Gavin, “The levenberg-marquardt algorithm for nonlinear least squares curve-fitting problems,” *Department of Civil and Environmental Engineering, Duke University*, pp. 1–19, 2019.
- [21] Q.-Y. Zhou, J. Park, and V. Koltun, “Fast global registration,” in *European conference on computer vision*. Springer, 2016, pp. 766–782.
- [22] T. Shan, B. Englot, D. Meyers, W. Wang, C. Ratti, and D. Rus, “Lio-sam: Tightly-coupled lidar inertial odometry via smoothing and mapping,” in *2020 IEEE/RSJ International Conference on Intelligent Robots and Systems (IROS)*. IEEE, 2020, pp. 5135–5142.
- [23] R. B. Rusu, N. Blodow, and M. Beetz, “Fast point feature histograms (fpfh) for 3d registration,” in *2009 IEEE international conference on robotics and automation*. IEEE, 2009, pp. 3212–3217.
- [24] J. Zhang and S. Singh, “Loam: Lidar odometry and mapping in real-time,” in *Robotics: Science and Systems*, vol. 2, no. 9. Berkeley, CA, 2014, pp. 1–9.